RSC Advances

PAPER

View Article Online
View Journal | View Issue

Cite this: *RSC Adv.*, 2014, **4**, 64457

Ultrastructure of metallopeptide-based soft spherical morphologies†

Gagandeep Kaur,[a] Lihi A. Abramovich,[b] Ehud Gazit*[b] and Sandeep Verma*[a]

Received 16th September 2014
Accepted 18th November 2014

DOI: 10.1039/c4ra10532j

www.rsc.org/advances

Peptides and proteins offer interesting starting points for triggering self-assembly processes owing to the chemical diversity of side-chains, ease of chemical modifications and the possibility of exploiting several non-covalent and metal-assisted interactions, to stabilize higher order ensembles. Consequently, a variety of nanoscale morphologies such as fibers, vesicles, nanotubes are observed for modified amino acids and short peptides and these biocompatible soft materials have been used for diverse biological, medical and material applications. Herein, we report metal-mediated modification of spherical soft assemblies, by introducing a coordinating linker for the Phe–Phe dipeptide, which results in the coalescence of soft structures. The possibility of copper ion coordination, with the metal-binding peptide conjugate, was confirmed by single crystal analysis. Based on these observations, a model depicting possible interactions leading to soft structure formation and metal-aided coalescence is also presented. The coalescence could be reversed in the case of Au-mediated soft structures with the help of thiol interference. Such an approach, exploiting interfacial metal ion interactions, is expected to provide an entry into novel metallopeptide materials.

Introduction

Self-assembling peptides offer a versatile platform towards formation of ordered nanoscale systems, with various applications in catalysis, delivery, and tissue engineering, to name a few.[1–8] Control through different physicochemical properties of constituent amino acids, possibility of predictable design based on secondary structural signatures, and high compatibility interaction with other biological systems, are the hallmarks of peptide-based nanoscale materials. Consequently, it is quite advantageous to employ short self-assembling peptides, to obtain diverse hierarchical structures with desired functions. Recent advances along these lines concern interaction of metal ions with self-assembling peptides to afford bio-inspired metal–peptide frameworks (MPF),[9,10] which may offer combined investigated properties of metal–organic frameworks (MOF) with biocompatibility.

Three different approaches could be envisaged for constructing MPFs: (i) introducing amino acids side chains capable of metal binding[11] (ii) use of exogenous ligands supporting MOF architecture[12] (iii) use of covalently linked chiral/achiral connectors. These approaches represent facile route for the design of novel, abiotic oligomers for supramolecular studies. As a specific example, Lehn, Huc and other groups have reported family of oligoamides based on achiral connectivity of 2,6-pyridinedicarboxylic acid, where the resultant oligomers not only self-organized into single helices, but also support formation of double helices under specific conditions.[13,14] Notably, short oligomers with 2,6-pyridinedicarboxylic acid and related connectors afford planar 'crescent-like' conformation, while longer oligomers exhibit more pronounced propensity to form helical structures.[15] In particular, pyridine diacid oligomers offer hydrogen bonding at the inner rim of helices resulting in ~4.5 monomer per turn of the ensuing helix.

Diphenylalanine (FF) dipeptide motif exhibits spontaneous self-assembly to generate peptide nanotubes in solution.[16] FF nanotubes offer interesting applications as scaffolds for the synthesis of metal nanowires, possess improved mechanical properties, semi-conductivity and serve as potential drug delivery agents.[17–23] Side chain aromaticity in phenylalanine is implicated for self-assembly properties and key structural features in the solid state.[24] In current study, given our continued interest in hierarchical self-assembled peptides systems and our ongoing efforts to prepare covalently linked conjugates of FF dipeptide,[18,25,26] we decided to synthesize a symmetric FF conjugate using pyridinedicarboxylic acid as an

[a]*Department of Chemistry, DST Thematic Unit of Excellence on Soft Nanofabrication, Center for Environmental Sciences and Engineering, Indian Institute of Technology Kanpur, Kanpur-208016, India*

[b]*Department of Molecular Biology and Biotechnology, Department of Materials Science and Engineering, Tel Aviv University, Tel Aviv-69978, Israel. E-mail: sverma@iitk.ac.in; ehudg@post.tau.ac.il*

† Electronic supplementary information (ESI) available: Crystallographic data, details structures showing H-bonding and CH···π interactions in $Cu_2\mathbf{4}_2$ complex. HR-SEM images of **4** + metal ions on copper grid and spectral characterisation. CCDC 1005702. For ESI and crystallographic data in CIF or other electronic format see DOI: 10.1039/c4ra10532j

achiral linker. The ability of this new peptide conjugate to self-assemble and its binding to various metals including copper, silver and gold leading to formation of metallopeptide soft structures is described.

Results and discussions

Molecular design of peptide conjugate, 4

We designed and synthesized **4**, which is a hybrid of two diphenylalanine moieties conjugated using 2,6-pyridinedicarboxylic acid as a linker (Scheme 1). We envisioned the following advantages for the proposed conjugate: [i] possibility to engender a structure containing the ability of 'crescent-like' conformation in an aggregating dipeptide (Fig. 1a); [ii] introduction of metal ion co-ordination sites to further interrogate peptide self-assembly process.

2,6-Pyridyl disubstituted linkers have been utilized to engender a crescent conformation or a curvature in many foldameric systems.[15,27] In addition, pyridyl ring also offers additional advantage of metal ion interaction, which may further lead to useful coordination architectures and varied geometries. It can thus be surmised that such curved conformation (Fig. 1), upon solution phase self-assembly, may eventually culminate into spherical structures.

Crystal structure of 4 with Cu ions

Presence of pyridyl group as a linker gave us an impetus to focus our attention to metal ion coordination. As envisaged, we surmised that such interaction may offer an entry metal-mediated peptide soft matter, perhaps with tunable size and cavities. To start, we decided to assess metal ion interaction by growing appropriate crystal to ascertain the possible site of metal binding. **4** was interacted with Cu(II) ions and studied through single-crystal diffraction analysis (Fig. 2a and Table S1†). Methanolic solution of **4** was treated with $CuSO_4 \cdot 5H_2O$

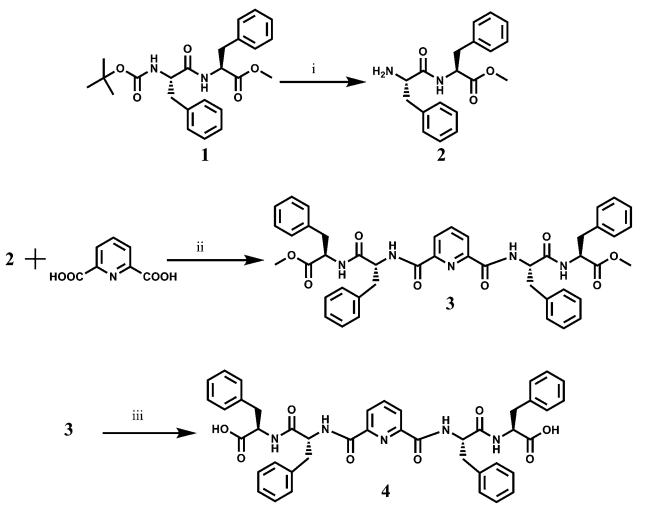

Scheme 1 Synthetic scheme of peptide conjugate **4**: (i) 75% TFA-DCM, 4 h, N_2 atm. (ii) HOBt, DCC, 0 °C, TEA, N_2 atm. (iii) THF, 1 N NaOH, 6 h, N_2 atm.

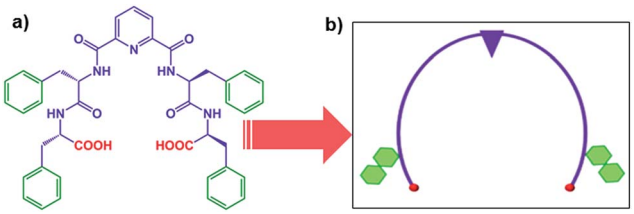

Fig. 1 (a) Molecular structure of **4**. (b) Predicted curvature of **4**.

and diffraction quality crystals were grown by slow evaporation method. Crystal analysis revealed M_2L_2 coordination, *via* carboxylate groups, to afford a Cu(II)-supported paddle-wheel like structure.[28–31] The dimeric units were further stabilized by hydrogen bonding between –N–H and –C=O of adjacent dimeric units in the range of 2.11–2.12 Å (Fig. S1a†) as well as through C–H$\cdots\pi$ interactions (2.47 Å)[32–35] (Fig. S1b†), to form a 3D lattice structure (Fig. 2b; Table S2†). Notably, Cu(II) ions in this case did not interact with pyridyl nitrogen.

Formation of M_2L_2-type of discreet dinuclear copper cluster evinces interest not only due to interesting coordination geometry, but also due to the fact that coordination-driven self-assembled structures offer facile entry to the construction of novel metallosupramolecular ensembles such as two-dimensional polygons and three-dimensional spherical cages, prisms, and polyhedral.[36–39] It is envisaged that these designed superstructures, which combine multiple weak interactions including π–π stacking, CH–π interactions, hydrogen bonds and metal-coordination, could extend application in domains ranging from optoelectronic materials to drug delivery to storage and catalysis. In case of **4**, it could be imagined from crystal structure that metal–carboxylate interactions offer a beneficial cooperative effect, along with other stabilizing non-covalent interactions, to form interesting superstructures. Thus, we started with the determination of solution-phase morphology of **4**, followed by investigating the effect of metal ions, in the solution phase, to generate metallopeptide ensembles.

Solution phase self-assembly of 4

The propensity of peptide conjugate **4** to self-assemble was studied. It was dissolved in 50% methanol–water at a concentration of 1 mM and unlike nanotube forming FF dipeptide,[16] **4** leads to instantaneous formation of spherical structures with a diameter of 350–650 nm, as confirmed by atomic force microscopy (AFM) (Fig. 3a and b) and dynamic light scattering (DLS) analysis (Fig. 3c). Spherical nature of these assemblies could be attributed to the crescent-shaped structural design of this conjugate. These spherical morphologies were further analysed using scanning electron microscopy (SEM) and transmission electron microscopy (TEM) (Fig. 3d and e).

Stability of these soft structures was probed by subjecting them to high-energy ion beam manipulation (Fig. 3f). Consequently, a focused ion beam (FIB) system, using a gallium ion beam, was employed to site-selectively machine a spherical particle, at an operating voltage of 15.00 kV. This experiment

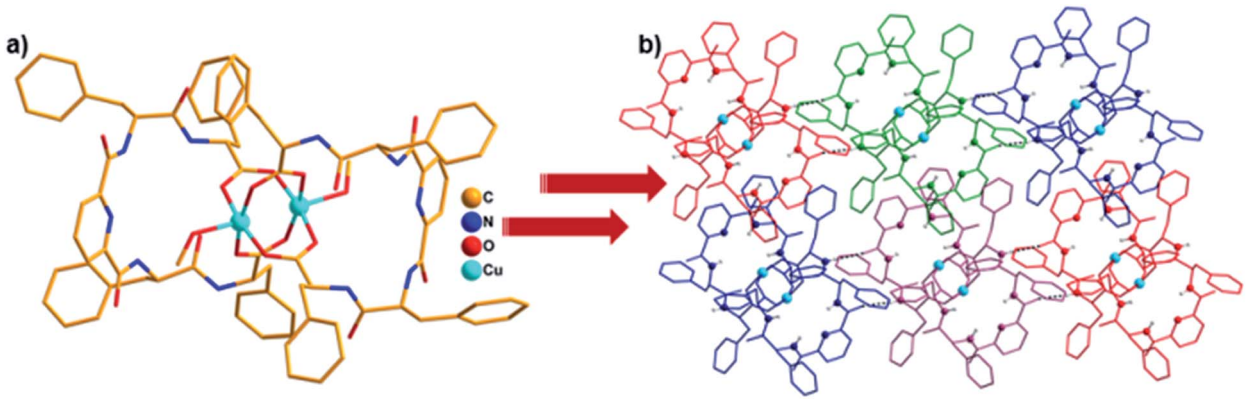

Fig. 2 Crystal structure of Cu_2L_2 metallopeptide (L = **4**): (a) dinuclear paddle wheel-type of structure (b) lattice structure showing peripheral interactions.

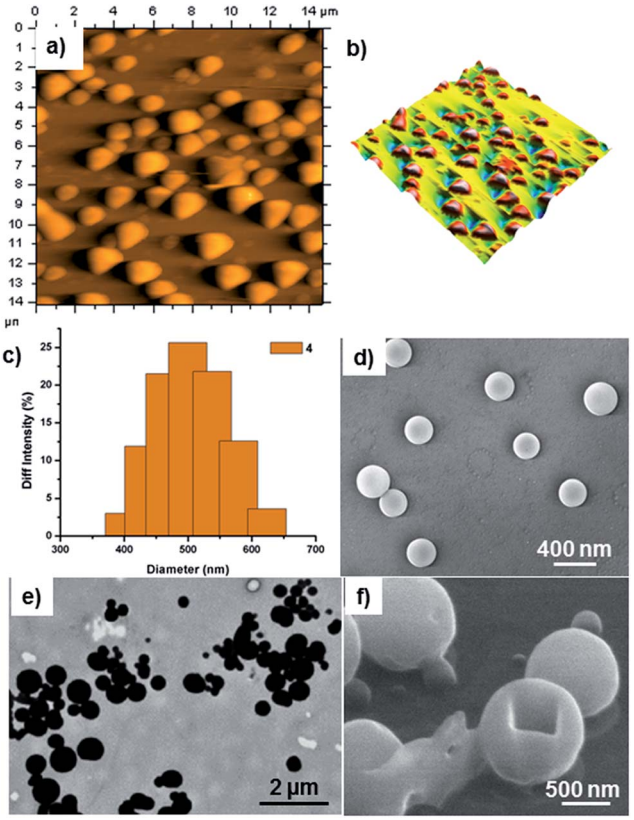

Fig. 3 Microscopy analysis of **4** (a and b) AFM micrographs. (c) DLS spectrum showing the spherical structure size distribution. (d) SEM image. (e) TEM image. (f) FIB-SEM image of the sphere after ion beam damage revealing the inner surface (1 mM, 50% aqueous methanol) on silicon wafer.

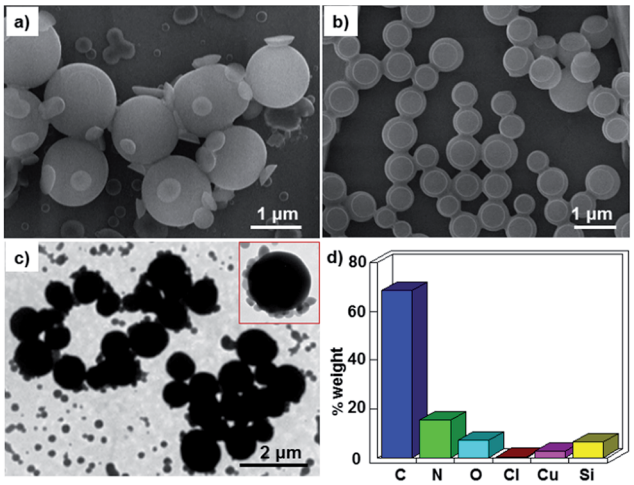

Fig. 4 Microscopic images of **4** + Cu(II) complex. (a and b) SEM images on silicon wafer after 12 h and 24 h respectively. (c) TEM image (inset: magnified view of a metal-bound spherical structure). (d) EDX spectrum after 24 h.

revealed a solid inner core in the soft structure, suggesting formation of highly compact structures that are able to withstand ion beams without any measurable loss of morphological integrity.[40]

Stabilization of these structures could be attributed to known aromatic amino acid side-chain interactions during peptide aggregation process to form parallel-stacked or T-shaped geometries. Such instances lead to formation of hydrophobic microenvironments by excluding water. Moreover, it is also known that aromatic–aromatic interactions further help short peptides to efficiently access energetically favored conformations.[41–44] It should be emphasized here that mixed solvent used in this case, due to solubility constraints, may also exert some effect in stabilizing FF dipeptide side-chain interactions. Notably, stacked arrangements are more stable in water, while amphiphilicity of methanol interferes with both stacked and T-shaped geometries, by attenuating aromatic–aromatic interactions.[45]

Interaction of 4 with copper ions

Cu(II) ions form stable four-, five- and six-coordinate complexes. These complexes show their potential use as anti-inflammatory,[46] antimicrobial,[47] antitumor agents,[48–51] enzyme inhibitors, and chemical nucleases, generally bind through nitrogen of the ligands. Conjugate **4** offers pyridyl ring nitrogen as well as free

carboxylate groups as probable metal binding sites. Samples were prepared by co-incubating **4** (1 mM, 0.5 mL, MeOH) with $CuCl_2 \cdot 2H_2O$ solution (1 mM, 0.5 mL, H_2O), followed by microscopy evaluation. Minor morphological changes appeared within 2 h of mixing, which became prominent during prolonged incubation as confirmed by SEM and TEM microscopy (Fig. 4). These images clearly showed vesicle coalescence in presence of metal ions, leading to the formation of larger-sized vesicles in 24 h (Fig. 4b). The monitoring was further continued for 120 h through DLS measurements. The size of spherical structures increased up to ~3.4 μm in 120 h upon copper interaction perhaps due to fusion of these vesicles. Notably, the presence of copper ions in vesicles was confirmed by energy-dispersive X-ray spectroscopy (EDX) measurements (Fig. 4d).

One of the hallmarks of Cu(II) interaction was the coalescence of self-assembled structures. As Phe–Phe interactions are primarily guided by stacking interactions, phenyl rings prefer to be buried inside the spherical structures. Thus, it is likely that free carboxylic groups and pyridyl ring nitrogens in **4** would possibly be exposed at the surface of spherical structures for metal ion binding.[52]

Interaction of 4 with silver ions

Ag(I) ions generally interact through nitrogen centers in the ligands[53] and many such complexes are known to exhibit biological activities.[54,55] They are also known to trigger conformational changes in self-assembled peptides.[56] As pyridyl nitrogen of **4** could be an interesting metal binding site for Ag(I), samples were prepared in presence of $AgNO_3$ as described before. We were able to observe changes in morphology 12 h after the addition of metal ions (Fig. 5a). Interestingly, coalescence of spherical vesicles was observed again, where soft structures of **4** exhibited formation of fused structures, as evidenced by SEM and TEM micrographs (Fig. 5b and c). As this morphology change was slightly different compared to copper-mediated morphology, it is possible that Ag(I) coordination in this case is distinct to Cu(II) interactions.[57]

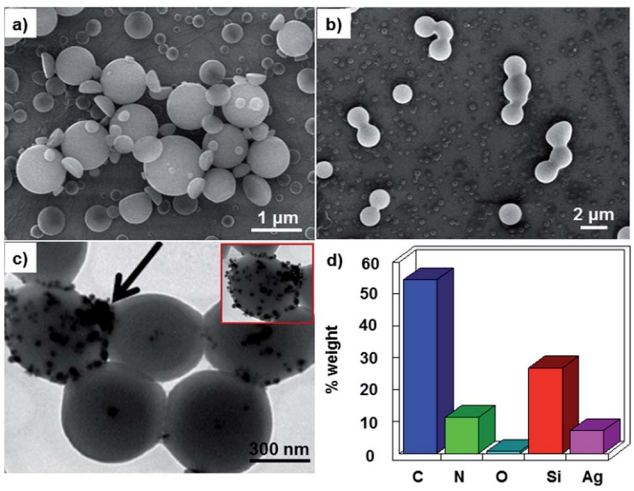

Fig. 5 Microscopic images of **4** + Ag(I) complex. (a and b) SEM images on silicon wafer after 12 h and 24 h respectively. (c) TEM image (inset: magnified view of a Ag(I)-mediated soft spherical structures). (d) EDX spectrum after 24 h.

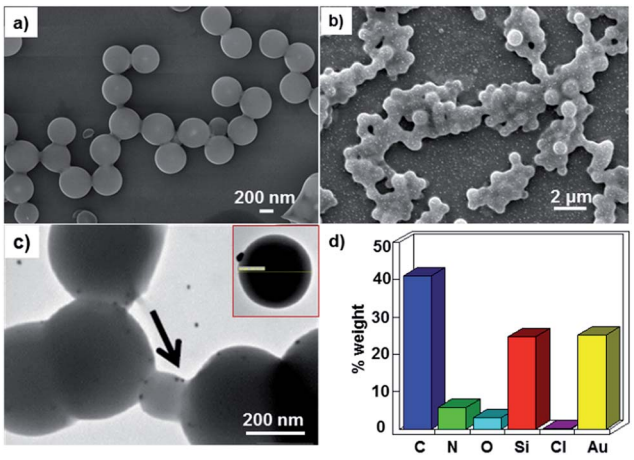

Fig. 6 Microscopic images of **4** + Au(III) complex. (a and b) SEM images on Si wafer after 12 h and 24 h respectively. (c) TEM image, (inset: magnified view of a spherical structure). (d) EDX spectrum after 24 h.

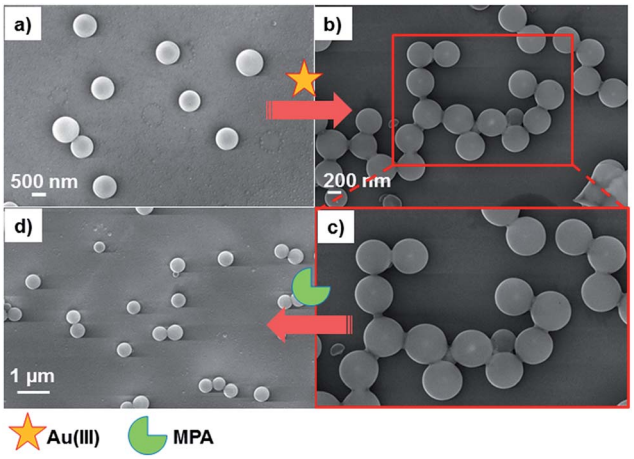

Fig. 7 (a) SEM image of **4**. (b) SEM image of **4** + Au(III) complex after 12 h. (C) Magnified view of **4** + Au(III) complex. (d) SEM image of **4** + Au(III) + MPA after 5 h incubation.

Unfortunately, our efforts to grow single crystals with Ag ions were not successful.

Interaction of 4 with Au(III) ions

Chloroauric acid ($HAuCl_4$) protonates pyridyl ring with counter anion $AuCl_4^-$ ion balancing overall charge.[58–61] Latter possesses square-planar geometry, relatively diffuse charge distribution and a weak interaction with solvent (water) molecules, with nearest solvent molecules occupying two orthogonal quasi-elliptical surfaces.[62] Dissolving **4** along with $HAuCl_4$ also revealed morphological changes, where spherical structures were found to afford a network-like morphology within 12 h incubation (Fig. 6). Given the anionic nature of $AuCl_4^-$, it is likely that carboxylate anions will not have any role in coordination. Thus, observed coalescence could be attributed to pyridyl nitrogen coordination of Au(III). Indeed, several groups have reported formation of Au(III) coordination complexes using

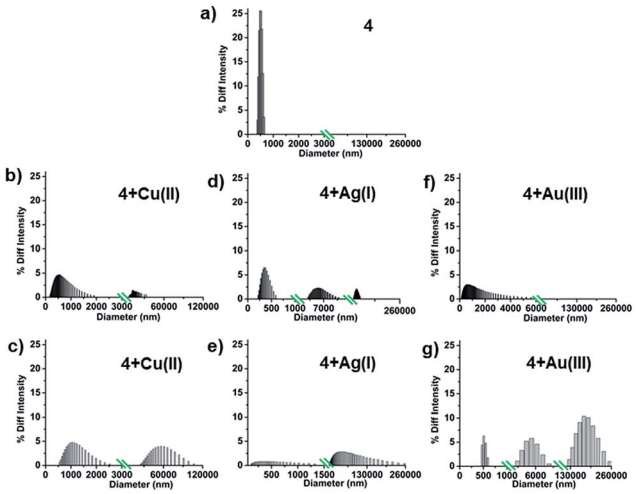

Fig. 8 DLS spectra: (a) size distribution of **4** (50% MeOH–H_2O). (b, d and f) Size distributions after 24 h. (c, e and f) Size distributions after 120 h.

pyridyl and phenanthronyl ligands.[63] Vesicles linked in a network-like fashion were confirmed by various microscopy methods and EDX analysis data.

Thus, different possibilities could be envisaged for metal–peptide interactions: in case of Cu(II) ions, free carboxyl group side-chains in **4** could interact as suggested by the solid state structure; but, this does not preclude solution interaction of pyridyl nitrogens with copper ions. In case of Ag(I) and Au(III) ions, interaction could possibly be supported by pyridyl nitrogen. Despite repeated attempts, we were unable to grow crystals with Ag(I) and Au(III) ions to arrive at precise sites of Ag or Au interaction with **4**. Finally, role of surface in these experiments was also probed by doing this procedure on copper grids (Fig. S2†). Similar results were obtained in all three cases irrespective of the surface used.

Thiol displacement studies

Au(III) ion binds very effectively with **4** to form network-like metal–peptide framework. As Au(III) has thiophilic binding preference over nitrogen or oxygen centers,[64,65] we decided to treat **4** + Au(III) complex with 1-mercaptopropanoic acid (MPA) to achieve its displacement from the framework. Samples were prepared by mixing **4** (0.5 mL, 1 mM, MeOH) with $HAuCl_4$ solution (0.5 mL, 1 mM, H_2O), incubated for 12 h. This was followed by addition of MPA solution (0.5 mL, 10 mM, 50% methanol–water) and further incubation of 5 h (Fig. 7). Notably, network-like structure disappeared confirming crucial role of Au(III) ions in causing metalized vesicles to stick together.

Dynamic light scattering analysis

Effect of metal ions on vesicle coalescence was confirmed by DLS analysis using similar metal–peptide solutions used for microscopy studies.[66] The samples were prepared by mixing **4** (1 mL, 10 μm, MeOH) with metal ion solutions (1 mL, 10 μm, H_2O). It was observed that the peptide vesicles alone have a hydrodynamic diameter of ~350–650 nm (Fig. 8a), which upon Cu(II) ions addition changes to ~1.2 μm (Fig. 8b) after 24 h incubation and it further matured to an average diameter of ~3.4 μm after 120 h (Fig. 8c). For Ag(I) ions, average size of metalated vesicles changed to ~1 μm after 24 h (Fig. 8d) and matured to an average diameter of 2.2 μm after 120 h (Fig. 8e). Similar trend was also observed for Au(III) interactions (Fig. 8f and g). Such a change in size may be ascribed to metal-mediated vesicle fusion process.

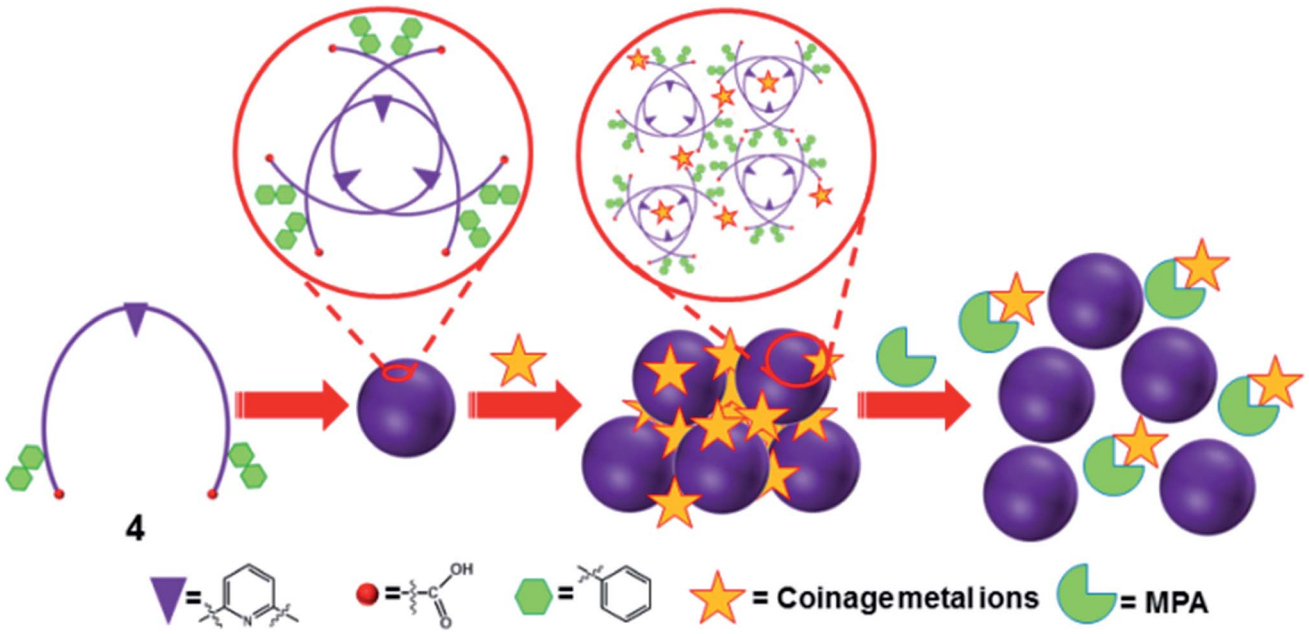

Fig. 9 Proposed model of metal–peptide interactions.

Peptide conjugate **4** afforded formation of spherical structures supported by H-bonding and π–π stacking interactions. Moreover, possible crescent-shape of monomers, engendered by pyridyl linker, further assisted self-organization of **4** to maximize non-covalent interactions.

Based on the occurrence of these forces, a model could be proposed to depict formation of spherical vesicles from crescent-shaped conjugate (Fig. 9). Observation of coalescence upon metal ion addition was attributed to metal-coordination, which could possibly bring these soft peptide-based structures in close proximity. As seen in Au experiment, exogenous addition of MPA could revert coalescence perhaps by complexing metal ions thus releasing spherical structures.

Conclusions

Conjugate **4** was designed having a crescent-type of structure, synthesized and studied for its interaction with metal ions in the solid state and in solution. Crystal analysis of copper complex of **4** revealed M_2L_2 coordination, *via* carboxylate groups, to afford a Cu(II)-supported paddle-wheel like structure. Lattice structure offered insight into further interactions of these dinuclear units *via* noncovalent interactions. Solution phase self-assembly peptide conjugate revealed formation of spherical structures, which possessed metal ion binding properties leading to coalescence, as confirmed by microscopy. Cu(II), Ag(I) and Au(III) to form large sized vesicles: while Cu(II) ions bound free acid side chains of **4** as confirmed by solid state structure, Ag(I) and Au(III) ions could also invoke pyridyl nitrogen as additional binding sites. Reversal of coalescence was achieved in the case of Au(III) ions supported metal–peptide structures, when treated with 1-mercaptopropanoic acid. Thus, it can be stated that metal coordination plays an important role in connecting these spherical structures and exploit an interesting interfacial interaction to provide expeditious entry into novel metallopeptide materials.

Materials and methods

General procedures

N,*N*′-Dicyclohexylcarbodiimide (DCC), *N*-hydroxybenzotriazole (HOBt), di-*tert*-butyl dicarbonate (Boc), trifluoroacetic acid (TFA), and L-phenylalanine were purchased from SRL, Mumbai, India and used without further purification. Dichloromethane (DCM), *N*,*N*-dimethylformamide (DMF), methanol (MeOH) and triethylamine (TEA) were distilled according to standard procedures prior to use. ^{1}H and ^{13}C NMR spectra were recorded on JEOL-DELTA2 500 model operating at 500 and 125 MHz, respectively. HRMS (ESI^+ and ESI^-) was recorded at IIT Kanpur, India, on WATERS, Q-Tof Premier Micromass HAB 213 mass spectrometer using capillary voltage 2.6–3.2 kV. IR spectra were recorded as KBr pellets on a Perkin-Elmer Model 1320 spectrophotometer operating from 400 to 4000 cm^{-1}. For thin layer chromatography (TLC), Merck pre-coated TLC plates (MEARK 60 F254) were used, and compounds were visualized with a UV light at 254 nm. Chromatographic separations were performed on S. D. Fine-Chem 100–200 mesh silica gel.

Synthesis of peptide conjugate

4 was prepared by solution phase peptide synthesis.

N-(*tert*-Butyloxycarbonyl)-L-phenylalanine-L-phenylalanine methyl ester (1)

N-(Boc)-L-phenylalanine (5 g, 18.8 mmol), and HOBt (2.55 g, 18.8 mmol) were dissolved in dry DMF (25 mL) under nitrogen atmosphere and the reaction mixture was cooled to 0 °C in an ice bath. A solution of DCC in DCM (4.66 g, 22.6 mmol) was then added drop wise to the reaction mixture. The reaction mixture was stirred at 0 °C for 1 h, after which, L-phenylalanine methyl ester hydrochloride (4.05 g, 22.6 mmol) was added to it followed by triethylamine (13.1 mL, 94.2 mmol). The reaction mixture was monitored and stirred for 24 h at room temperature under nitrogen atmosphere. Reaction mixture was concentrated *in vacuo*, redissolved in ethyl acetate and filtered to remove DCU. The organic layer was then washed with 1 N HCl (3 × 30 mL), 10% $NaHCO_3$ (3 × 30 mL) and brine (30 mL). The organic layer was dried over anhydrous sodium sulfate and concentrated *in vacuo*. The crude compound was purified through silica gel column chromatography by using hexane and ethyl acetate (80 : 20) solvent system to isolate pure **1** (6.17 g, 76.76% yield). m.p. 102–105 °C, Rf [30% ethyl acetate in hexane] = 0.5, ^{1}H NMR (500 MHz, $CDCl_3$, TMS, δ ppm): 1.38 (s, 9H); 2.99–3.08 (m, 4H); 3.65 (s, 3H); 4.32 (m, 1H); 4.77–4.93 (m, 1H); 6.96–6.97 (m, 2H); 7.17–7.29 (m, 10H, overlapped aromatic signal and $CDCl_3$ peak); ^{13}C NMR (125 MHz; $CDCl_3$, δ ppm): 28.3, 38.0, 38.3, 52.3, 53.3, 55.7, 77.3, 80.4, 127.2, 128.6, 128.7, 129.3, 129.4, 170.8, 171.4; HRMS $(M + H)^+$ for $C_{24}H_{30}N_2O_5$: 427.2233 (calcd), 427.2236 (anal.).

L-Phenylalanine-L-phenylalanine methyl ester (2)

1 (5 g, 9.5 mmol) was dissolved in 75% TFA-DCM and stirred for 1 h under nitrogen atmosphere. After completion of the reaction, the solvent was evaporated *in vacuo* and was subsequently washed with diethylether resulting in a white solid. The white solid then dissolved in methanol and passed through activated anion exchange resin and evaporated under reduced pressure to obtain pure **2** (3.27 g, 85.4% yield). Rf [50% ethyl acetate in hexane] = 0.5; ^{1}H NMR (500 MHz, DMSO-d_6, TMS, δ ppm): 2.89–3.09 (m, 4H), 3.57 (s, 3H); 4.02 (m, 1H); 4.51–4.55 (m, 1H); 7.18–7.30 (m, 10H), 8.16 (s, 3H); ^{13}C NMR (125 MHz; DMSO-d_6, δ ppm): 39.8, 40.0, 40.1, 40.3, 52.2, 54.1, 54.3, 128.4, 128.7, 129.5, 162.8, 172.1; HRMS $(M + H)^+$ for $C_{19}H_{22}N_2O_3$: 327.1709 (calcd), 327.1700 (anal).

Pyridyl-bis-L-phenylalanine-L-phenylalanine methyl ester (3)

2,6-Pyridinedicarboxylic acid (0.25 g, 1.49 mmol) was dissolved in DMF and cooled to 0 °C in ice bath under nitrogen atmosphere. To this solution, HOBt (0.404 mg, 2.99 mmol) and a solution of DCC (0.617 g, 2.99 mmol) in DCM was added and stirred for 1 h under nitrogen atmosphere at 0 °C. Subsequently **2** (1.07 g, 3.29 mmol) was added into the reaction mixture followed by triethylamine (0.76 mL, 9.48 mmol). The reaction mixture was monitored and stirred for 24 h at room

temperature under nitrogen atmosphere. Reaction mixture was concentrated *in vacuo*, redissolved in ethyl acetate and filtered to remove DCU. The organic layer was then washed with 1 N HCl (3 × 30 mL), 10% $NaHCO_3$ (3 × 30 mL) and brine (30 mL). The organic layer was dried over anhydrous sodium sulfate and concentrated *in vacuo*. Crude compound was then purified through silica gel column chromatography by using methanol–DCM (4 : 96) resulting in pure **3**. (0.45 g, 38.5% yield). m.p. = 142–144 °C, Rf [5% methanol in DCM] = 0.5; ^{1}H NMR (500 MHz, DMSO-d_6, TMS, δ ppm) = 2.46–3.18 (m, 8H), 3.54 (s, 6H), 4.48–4.53 (m, 2H), 4.70–4.77 (m, 2H), 7.08–7.29 (m, 20H) 8.07 (m, 2H), 8.59–8.60 (m, 1H), 8.92–8.93 (2s, 4H); ^{13}C NMR (125 MHz; DMSO-d_6, δ ppm): 37.1, 37.8, 39.5, 40.0, 40.4, 40.5, 52.3, 54.3, 54.7, 125.2, 126.8, 127.0, 128.7, 137.5, 139.9, 149.0, 163.5, 170.3, 172.1; HRMS $(M + Cl)^-$ for $C_{45}H_{45}ClN_5O_8$: 818.2957 (calcd), 818.2957 (anal.).

Pyridyl-bis-L-phenylalanine-L-phenylalanine conjugate (4)

3 (0.1 g, 0.127 mmol) was dissolved in tetrahydrofuran to form a clear solution. To this 1 N NaOH (0.03 g, 0.765 mmol) was added and stirred for 6 h at room temperature. The solution obtained was passed over activated cation exchange resin. The filtrate was evaporated under reduced pressure to obtain pure **4**. (0.07 g, 72.9% yield); m.p. 120–122 °C; ^{1}H NMR (500 MHz, DMSO-d_6, TMS, δ ppm): 2.46–3.34 (m, 8H), 4.46–4.73 (m, 2H), 4.74–4.83 (m, 2H), 7.06–7.34 (m, 20H), 8.12–8.13 (m, 1H), 8.41–8.46, (m, 2H), 8.85–8.95 (m, 4H), 9.23–9.31 (m, 2H); ^{13}C NMR (125 MHz; DMSO-d_6, δ ppm): 37.1, 37.4, 39.5, 40.0, 40.2, 40.3, 54.3, 55.5, 125.3, 126.7, 126.9, 128.6, 129.6, 139.0, 148.9, 157.1, 163.9, 171.8, 173.4; FTIR (KBr, cm^{-1}): 1220, 1528, 1655 (C═O, amide I, II and III), 1736 (C═O, acid), 2931 (CH-aliph.), 3029 (CH-Ar), 3310 (NH, str); HRMS $(M - H)^-$ for $C_{43}H_{41}N_5O_8$: 754.2877 (calcd), 754.2877 (anal).

Field emission scanning electron microscopy (FE-SEM)

10 μL aliquots of the samples (1 mM in 50% methanol–water) were deposited on a silicon wafer (100) and allowed to dry at room temperature. Subsequently the samples were dried *in vacuo* for 30 min prior to imaging. The samples were imaged with and without (for EDX) gold coating. SEM images were acquired on FEI Quanta 200 microscope, equipped with a tungsten filament gun, operating at WD 3 mm and 10 kV.

Atomic force microscopy (AFM)

10 μL aliquots of samples (1 mM in 50% methanol–water) was placed on a silicon wafer (100) at room temperature and allowed to dry by slow evaporation. Subsequently the samples were dried *in vacuo* for 30 min prior to imaging. AFM Samples were imaged with an atomic force microscope (Molecular Imaging, USA) operating under the Acoustic AC mode (AAC), with the aid of a cantilever (NSC 12(c) from MikroMasch). The force constant was 0.6 N m^{-1}, while the resonant frequency was 150 kHz. The images were taken at room temperature, with the scan speed of 1.5–2.2 lines per s. The data acquisition was done using Pico-View 1.4® software, while the data analysis was done using PicoView.

Focused ion beam-scanning electron microscopy (FIB-SEM)

10 μL aliquots of the samples (1 mM in 50% methanol–water) were deposited on a silicon wafer (100) and allowed to dry at room temperature. Subsequently the samples were dried *in vacuo* for 30 min prior to imaging. FIB-SEM images were acquired on FEI make Nova 600 Nanolab workstation equipped with a field emission Ga ion source, operating at 15 kV.

Transmission electron microscopy (TEM)

10 μL aliquots of the sample (1 mM in 50% methanol–water) were placed on a 400-mesh copper grid. After 1 min any excess fluids were removed. Due to the present of metal samples were imaged without any further staining. Samples were viewed using a JEOL 1200EX electron microscope operating at 80 kV.

Dynamic light scattering (DLS)

Particle size distribution of **4**, **4** + Cu(II), **4** + Ag(I) and **4** + Au(III) complexes were measured using dynamic light scattering analyzer at a wavelength 657 nm, with Delsa Nano C Particle analyzer (Beckman Coulter). Samples were measured at 25 °C.

Acknowledgements

We thank Ion Beam Centre, Nuclear Physics unit, IIT Kanpur, for FIB-SEM and DST Thematic Unit of Excellence in Soft Nanofabrication, IIT Kanpur, for FE-SEM and DLS. We thank Z. Barkay for help with the SEM analysis and Y. Delarea for help with TEM experiments. We thank member of the Gazit group for helpful discussions. G.K. thanks IIT Kanpur and UGC, India for financial support. This work is supported by an Outstanding Investigator Award to S.V. from DAE-SRC, Department of Atomic Energy, India, J. C. Bose National Fellowship, DST, India, and by MHRD supported Centre for Excellence in Chemical Biology, IIT Kanpur.

Notes and references

1 D. W. Pack, A. S. Hoffman, S. Pun and P. S. Stayton, *Nat. Rev. Drug Discovery*, 2005, **4**, 581–593.
2 X. Guo and F. C. Szoka, *Acc. Chem. Res.*, 2003, **36**, 335–341.
3 O. S. Rabotyagova, P. Cebe and D. L. Kaplan, *Biomacromolecules*, 2011, **12**, 269–289.
4 J. D. Brodin, X. I. Ambroggio, C. Tang, K. N. Parent, T. S. Baker and F. A. Tezcan, *Nat. Chem.*, 2012, **4**, 375–382.
5 M. C. Branco and J. P. Schneider, *Acta Biomater.*, 2009, **5**, 817–831.
6 R. Hirst, B. Escuder, J. F. Miravet and D. K. Smith, *Angew. Chem., Int. Ed.*, 2008, **42**, 8002–8018.
7 E. F. Banwell, E. S. Abelardo, D. J. Adams, M. A. Birchall, A. Corrigan, A. M. Donald, M. Kirkland, L. C. Serpell, M. F. Butler and D. N. Wollfson, *Nat. Mater.*, 2009, **7**, 596–600.
8 Z. S. Al-Ahmady, W. T. Al-Jamal, J. V. Bossche, T. T. Bui, A. F. Drake, A. J. Mason and K. Kostarelos, *ACS Nano*, 2012, **6**, 9335–9346.

9 C. Mart-Gastaldo, J. E. Warren, K. C. Stylianou, N. L. O. Flack and M. J. Rosseinsky, *Angew. Chem., Int. Ed.*, 2012, **51**, 11044–11048.
10 C. Martí-Gastaldo, D. Antypov, J. E. Warren, M. E. Briggs, P. A. Chater, P. V. Wiper, G. J. Miller, Y. Z. Khimyak, G. R. Darling and N. G. Berry, *Nat. Chem.*, 2014, **6**, 343–351.
11 A. Mantion, L. Massüger, P. Rabu, C. Palivan, L. B. McCusker and A. Taubert, *J. Am. Chem. Soc.*, 2008, **130**, 2517–2526.
12 Y. Ikezoe, G. Washino, T. Uemura, S. Kitagawa and H. Matsui, *Nat. Mater.*, 2012, **11**, 1081–1085.
13 V. Berl, I. Huc, R. G. Khoury, M. J. Krische and J. M. Lehn, *Nature*, 2000, **407**, 720–723.
14 V. Berl, I. Huc, R. G. Khoury and J. M. Lehn, *Chem.–Eur. J.*, 2001, **7**, 2810–2820.
15 H. Jiang, J. M. Léger, C. Dolain, P. Guionneau and I. Huc, *Tetrahedron*, 2003, **59**, 8365–8374.
16 M. Reches and E. Gazit, *Science*, 2003, **300**, 625–627.
17 R. Ischakov, L. Alder-Abramovich, L. Buzhansky, T. Shekhter and E. Gazit, *Bioorg. Med. Chem.*, 2013, **21**, 3517–3522.
18 S. Ghosh, L. Alder-Abramovich, E. Gazit and S. Verma, *Tetrahedron*, 2013, **69**, 2004–2009.
19 R. J. A. Hill, V. L. Sedman, S. Allen, P. M. Williams, M. Paoli, L. Alder-Abramovich, E. Gazit, L. Eaves and S. J. B. Tendler, *Adv. Mater.*, 2007, **19**, 4474–4479.
20 M. Reches and E. Gazit, *Nat. Nanotechnol.*, 2006, **1**, 195–200.
21 L. Alder-Abramovich, N. Kol, I. Yanai, D. Barlam, R. Z. Shneck, E. Gazit and I. Rousso, *Angew. Chem., Int. Ed.*, 2010, **49**, 9939–9942.
22 L. Alder-Abramovich, D. Aronov, P. Beker, M. Yevnin, S. Stempler, L. Buzhansky, G. Rosenman and E. Gazit, *Nat. Nanotechnol.*, 2009, **4**, 849–854.
23 C. A. Hauser and S. Zhang, *Nature*, 2010, **468**, 516–517.
24 H. C. Görbitz, *Chem.–Eur. J.*, 2001, **7**, 5153–5159.
25 S. Mondal, A. K. Barman and S. Verma, *Chimia*, 2012, **66**, 930–935.
26 N. Gour, A. K. Braman and S. Verma, *J. Pept. Sci.*, 2012, **18**, 405–412.
27 D. W. Zhang, X. Zhao, J. L. Hou and T. Li, *Chem. Rev.*, 2012, **112**, 5271–5316.
28 A. Pichon, C. M. Fierro, M. Nieuwenhuyzen and S. L. James, *CrystEngComm*, 2007, **9**, 449–451.
29 J. S. Zhao, R. L. Zhang, S. Y. Yang and S. W. Ng, *Acta Crystallogr., Sect. E: Struct. Rep. Online*, 2004, **60**, m264–m266.
30 H. T. Xia, Y. F. Liu and S. A. Li, *Acta Crystallogr., Sect. E: Struct. Rep. Online*, 2006, **62**, m2653–m2655.
31 L. L. Kong, L. H. Huo, S. Gao and J. G. Zhao, *Acta Crystallogr., Sect. E: Struct. Rep. Online*, 2005, **61**, m2289–m2290.
32 A. Otero, A. Lara-Sánchez, J. Fernández-Baeza, C. Alonoso-Moreno, J. Tejeda, A. Castro-Osma, I. Márquez-Segovia, L. F. Sánchez-Barba, A. M. Rodríguez and M. V. Gómez, *Chem.–Eur. J.*, 2010, **16**, 8615–8619.
33 M. Nishio, *CrystEngComm*, 2004, **6**, 130–158.
34 J. Kumar, C. S. Purohit and S. Verma, *Chem. Commun.*, 2008, 2526–2528.
35 S. Bracco, A. Comotti, P. Valsesia, M. Beretta and P. Sozzani, *CrystEngComm*, 2010, **12**, 2318–2321.
36 T. R. Cook, Y. R. Zheng and P. Stang, *Chem. Rev.*, 2013, **113**, 734–777.
37 M. Spokoyny, D. Kim, A. Sumrein and C. A. Mirkin, *Chem. Soc. Rev.*, 2009, **38**, 1218–1227.
38 G. H. Clever, W. Kawamura, S. Tashiro, M. Shiro and M. Shionoya, *Angew. Chem., Int. Ed.*, 2012, **51**, 2606–2609.
39 A. Carné-Sánchez, I. Imaz, M. Cano-Sarabia and D. A. Maspoch, *Nat. Chem.*, 2013, **5**, 203–211.
40 K. B. Joshi and S. Verma, *Angew. Chem., Int. Ed.*, 2008, **47**, 2860–2863.
41 E. Gazit, *FEBS J.*, 2005, **272**, 5971–5978.
42 E. Gazit, *FASEB J.*, 2002, **16**, 77–83.
43 M. L. Waters, *Curr. Opin. Chem. Biol.*, 2002, **6**, 736–741.
44 E. Gloaguen, Y. Loquais, J. A. Thomas, D. W. Pratt and M. Mons, *J. Phys. Chem. B*, 2013, **117**, 4945–4955.
45 R. Chelii, F. L. Gervasio, P. Procacci and V. Schettino, *J. Am. Chem. Soc.*, 2002, **124**, 6133–6143.
46 T. Chaviara, P. C. Charistidis, A. Papageorgiou, E. Chrysogelou, J. Hadjipavlou-Litina and C. A. Bolos, *J. Inorg. Biochem.*, 2005, **99**, 2102–2109.
47 K. Y. Djoko, B. M. Paterson, P. S. Donnelly and A. G. McEwan, *Metallomics*, 2014, **6**, 854–863.
48 N. H. Gokhale, S. S. Padhye, S. B. Psdhye, C. E. Anson and A. K. Powell, *Inorg. Chim. Acta*, 2001, **319**, 90–94.
49 Z. Trávníček, M. Maloň, Z. Šindelář, K. Doležal, J. Rolčík, V. Kryštof, M. Strnad and J. Marek, *J. Inorg. Biochem.*, 2001, **84**, 23–32.
50 A. Marín-Hernández, I. Gracia-Mora, L. Ruiz-Ramírez and R. Moreno-Sánchez, *Biochem. Pharmacol.*, 2003, **65**, 1979–1989.
51 M. Barceló-Oliver, Á. Garcia-Raso, Á. Terrón, E. Molins, M. J. Prieto, V. Moreno, J. Martínez, V. Lladó, I. López and A. Gutiérrez, *J. Inorg. Biochem.*, 2007, **101**, 649–659.
52 S. M. Butterfield, P. R. Patel and M. L. Waters, *J. Am. Chem. Soc.*, 2002, **124**, 9751–9755.
53 T. Hu and T. C. W. Mak, *Eur. J. Inorg. Chem.*, 2013, 5476–5486.
54 N. Gerasimchuk, A. Gamian, G. Glover and B. Szponar, *Inorg. Chem.*, 2010, **49**, 9863–9874.
55 F. F. Fan and A. J. Bard, *J. Phys. Chem. B*, 2002, **106**, 279–287.
56 S. N. Dublin and V. P. Conticello, *J. Am. Chem. Soc.*, 2008, **130**, 49–51.
57 P. Halder, E. Zangrando and T. P. Paine, *Dalton Trans.*, 2009, 5386–5394.
58 J. P. Spatz, S. Sheiko and M. Moller, *Macromolecule*, 1996, **29**, 3220–3226.
59 J. P. Spatz, S. Mossmer, C. Hartmann and M. Moller, *Langmuir*, 2000, **16**, 407–415.
60 X. Li, S. Zhao, S. Zhang, D. H. Kim and W. Knoll, *Langmuir*, 2007, **23**, 6883–6888.
61 S. N. Sidorov, L. M. Bronstein, Y. A. Kabachii, P. M. Valetsky, P. L. Soo, D. Maysinger and A. Eisenberg, *Langmuir*, 2004, **20**, 3543–3550.
62 Q. Ye, J. Zhou, T. Zhao, H. Zhao, W. Chu, Z. Sheng, X. Chen, A. Marcelli, Y. Luo and Z. Wu, *J. Phys. Chem. B*, 2012, **116**, 7866–7873.

63 Z. D. Hudson, C. D. Sanghvi, M. A. Rhine, J. J. Ng, S. D. Bunge, K. I. Hardcastle, M. R. Saadein and C. E. MacBethc, *Dalton Trans.*, 2009, 7473–7480.
64 T. A. Rodina, A. V. Ivanov, A. V. Gerasimenko, O. V. Loseva, O. N. Antzutkin and V. I. Sergienko, *Polyhedron*, 2012, **40**, 53–64.
65 J. M. Tunny, A. J. Blake, E. S. Davies, J. McMaster, C. Wilson and C. D. Garner, *Polyhedron*, 2006, **25**, 591–598.
66 H. Jin, W. Huang, Y. Zheng, Y. Zhou and D. Yan, *Chem.–Eur. J.*, 2012, **18**, 8641–8646.